Research Journal of Applied Sciences, Engineering and Technology 14(11): 436-444, 2017
DOI:10.19026/rjaset.14.5145
ISSN: 2040-7459; e-ISSN: 2040-7467

Submitted: August 8, 2017 Accepted: September 11, 2017 Published: November 15, 2017

Research Article

An Experimental and Theoretical Investigation into Deformation of Internally-Spline Sleeves

[1]Ayman A. Abd-Eltwab, [2]S.Z. El- Abden, [3]Khaled I.E. Ahmed, [1]M.N. El-Sheikh and [1]Ragab K. Abdel-Magied
[1]Mechanical Engineering Department, Beni-Suef University, Beni-Suef,
[2]Prod. Engineering and Design Department, Minia University, El Minia,
[3]Mechanical Engineering Department, Assiut University, Assiut, Egypt

Abstract: The aim of this research is to investigate experimentally and theoretically the parameters affecting on the deformation of internally-spline sleeves manufactured by ball spinning tool. Internally-spline sleeves have an increased attention since these parts serve as power transmission means in many industrial applications. The process was investigated experimentally and theoretically for commercial Aluminum tubes. The experimentally investigated variables were: the rotational speed of the mandrel 76, 150, 230 and 305 rpm; the axial feed, 0.3, 0.6, 0.9 and 1.21 mm/ rev; the cross in-feed 1.5, 2, 2.5 and 3 mm. An analytical expression was derived to predict the deformation loads. The theoretically investigated variables were: the mentioned axial feed and cross in-feed at 230 mandrel rotational speed. The effects of these variables on the forming load and the quality of formed sleeves were investigated. The results showed that, these variables affect the forming load and product quality. The optimum values of these variables were determined. The theoretical results with pile up have been found to be in close agreement with the experimental results.

Keywords: Analytical model, ball spinning, internally-spline sleeves, process parameters, product quality, shear spinning

INTRODUCTION

Tubular parts with longitudinal inward ribs, interior sections and inside splines rise so as to adjust to the advancement of flight related, aviation and military industries (Ahmed, 2011). The tubular parts can be fabricated by traditional techniques. Such parts with inner ribs are created by machining the billet by forging or casting which brings inadequacies of high material utilizing, high-vitality utilization and low efficiency (Wong *et al*., 2003). Deformation processes also can be used to manufacture these parts by ballizing technique (Prakash and Singhal, 1995). The ballizing system is one of shear spinning or tube spinning forms. Ballizing tube spinning is generally utilized as a part of producing tubular parts with inward splines (Shu-Yong *et al*., 2006). Tube spinning is not just known for low load limit and low manufacturing cost, additionally is known for producing parts with high mechanical properties and smooth surface utilizing straightforward tooling (El-Sheikh, 1991). In recent years, several attempts have been devoted towards the utilization of ball's for burnishing of internal cylindrical surface, external cylindrical surface, lap joining of tubes and rotary ball squeezing. In practice, shaping and broaching are the basic alternative processes commonly used for the manufacturing of splined sleeves. Time-consuming preparations, material saving, mechanical properties of the soft material improving for a four-mentioned manufacturing processes and high cost for the special splines machines are the obvious demerits of this technique. The main advantages of the manufacturing by spinning processes are low forming loads, simple tooling, good dimensional accuracy, low material utilization, low production costs, improved mechanical properties and low power consumption. Such processes were widely used to produce the tubular parts with internal ribs (Prakash and Singhal, 1995; Hayama, 1966). Tube spinning demonstrated great capacity of delivering microgroove blade inside tubes that used to upgrade the heat exchange and capillary geometry in micro-heat pipes (Tang *et al*., 2007).

For the most part, the last result of tube spinning process-utilizing balls is predominantly influenced by

Corresponding Author: Ayman A. Abd-Eltwab, Mechanical Engineering Department, Beni-Suef University, Beni-Suef, Egypt, Tel.: 00201005728351; Fax: 0020822241932

diameter of forming ball, thickness reducing per pass and the ductility of formed tube. Same properties were found for inward grooved tubes. The development of the inward ribs starts at certain basic ball size, after which, the height of the shaped ribs increments with the increasing of the ball diameter (Jiang *et al*., 2009a). This connection can control the tube dimensional precision and surface quality, which are essentially corrupted with the increase of the ball diameter (Jiang *et al*., 2009b). The inward ribs can't be formed without decreasing the tube thickness. The tallness of the shaped ribs increments with the increase of the tube thickness decrease per pass. Same behavior was found for formed tube material ductility (Groche and Fritsche, 2006). In any case, the unpredictability of the ball spinning process deformation mechanism is due to the continuity and localization of the process. The knowledge of the effect of process parameters such as friction characterization, material properties and workpiece geometry on the process mechanics will lead to enhancement in the design of the die and the equipment adequately and will foresee and keep the process of deformities. Kuss and Buchmayr (2016) examined limiting the defects amid ball spinning process and they gives a point by point see into a measurable plan of trials, The outcomes demonstrated a trend to increase the axial feed rate for a damage minimized process design. Liu and Wang (2013) investigated the forming laws and optimization forming process parameters of tube spinning with inner grooved, the effect of the different forming conditions was analyzed by using the method of orthogonal design based on the inner-grooved copper tubes (φ7.00×0.24). The results show that the motor and drawing speed should be controlled about 23000 r/min and 15 m/min respectively and the spinning position should be located at about 1.5 mm away from the center of the inner-grooved core head.

In this study, an experimentally and theoretically investigation was carried out to produces the tubular parts with internal ribs (internally-splined sleeves). The forming process was performed by forcing the metallic tube between steel balls mounted around the splined mandrel. The specimen will be formed internally and elongated according to the mandrel cavity. Variables investigated in this study were the cross in-feed 1.5, 2, 2.5 and 3.5 mm; the axial feed 0.3, 0.6, 0.91 and 1.21 mm/rev. The rotational splined mandrel speed 76, 185, 230 and 305 rpm; and the thickness of the tube which 4, 5, 6 and 7 mm. Tube material was commercial Aluminum, the influence of these variables on the forming load and quality of the sleeve were investigate.

MATHEMATICAL ANALYSIS

In the deforming process, each ball center has three motions; radial motion in Y-direction, rotational motion around Z-axis and axial motion in Z-direction. Due to these motions, the balls squeeze the tube specimen forming a contact area between balls and specimen. The contact area increases with deformation due to material piled up in front of balls (Fig. 1).

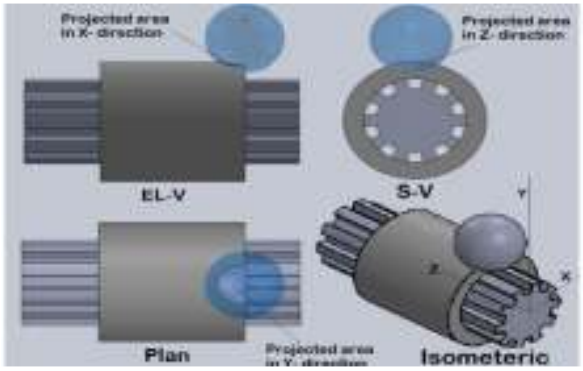

Fig. 1: Threecomponents of projected area.

The loads (FT) required for deformation, can be analyzed in three components (FX, FY and FZ components). These loads fill ribs with the metal and elongate the specimen in z- direction. These loads are divided into two parts; coining load required to force the material to fill the mandrel splines and spinning load required to make shear flow of external sleeve metal layers. The calculation process was based on the following assumptions:

- The strain hardening variation during the forming process can be neglected
- The spring back effect can be neglected
- The spinning material is homogenous, isotropic and incompressible
- Speed effect and temperature effect can be neglected during the deformation
- The load required to achieve the squeezing process is divided into two parts:
- Load required forcing the material for filling the mandrel splines (partial coining process)
- Load required for shear flow of external sleeve external layer (spinning process)

The three loads components are namely tangential force (FX), the radial force (FY) and the axial force (FZ); each component can be divided into coining and spinning load. The calculation of these loads are given by:

$$F_X = F_{XI} + F_{XII} \quad (1)$$

$$F_Y = F_{YI} + F_{YII} \quad (2)$$

$$F_Z = F_{ZI} + F_{ZII} \quad (3)$$

$$F_T = \sqrt{F_X{}^2 + F_Y{}^2 + F_Z{}^2} \quad (4)$$

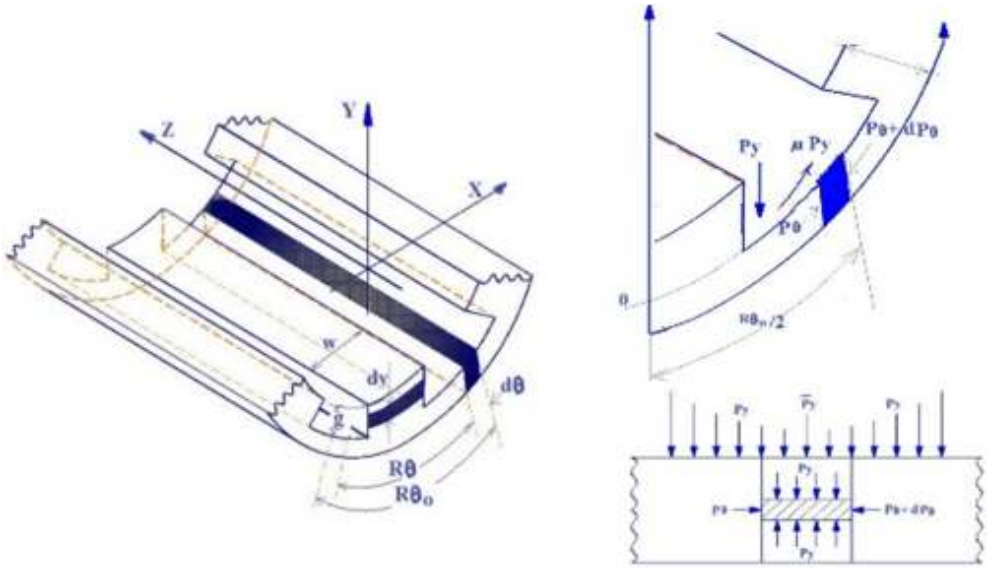

Fig. 2: Sections through splined sleeve

Using the slab method of stress analysis for the coining part of the load

Assumed that the stress distribution on any element of thickness to and width dRθ is uniform as shown in Fig. 2. duy/dy = constant, hence the strain rate ε = constant throughout the thickness to. This implies that the deviatorial stress must also be a constant. With compressive stress Pθ must be constant at any Rθ throughout to. Hence PY is permitted to vary along Rθ only on the central plane of the splined sleeve sector and is not a function of y.

The equilibrium consideration under the uniform state of stress shown in Fig. 2 on an arbitrary strip at Rθ having superimposed frictional stress μPY along the mandrel spline segment results in the differential equation in plane strain:

$$\frac{dP_\theta}{P_y} = \frac{2\,\mu}{t_o} dR_\theta \tag{5}$$

The metal flow has two dimensions; in the circumferential θ and perpendicular Y directions. Under the condition of plane strain the instantaneous yield condition or effect stress $\bar{\sigma}$ is given by:

$$\bar{\sigma} = \sqrt{\frac{3}{4}\left((P_y - P_\theta)^2\right)} \tag{6}$$

If $\bar{\sigma}$ is assumed not to be a function of θ, assuming uniform deformation, the differentiation of Eq. (6) yields:

$$dP_\theta = dP_y \tag{7}$$

Assumed that the data of stress in sleeve segment below the splines shown in Fig. 2 is constant. The

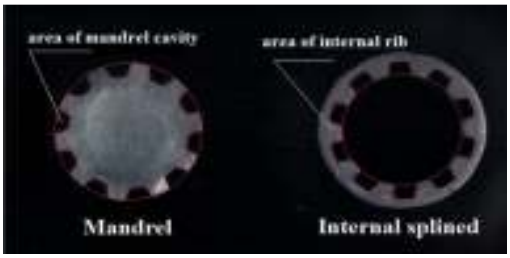

Fig. 3: Photo scan for mandrel and internal splined sleeve products to compute the filling ratio

pressure PY in the sleeve segment is equal to the pressure $\bar{P}$ resulting from frictional drag as the metal moves into the splines. Hence the instantaneous yield condition is given by:

$$P_\theta = \bar{P}_y + \frac{2}{\sqrt{3}}\bar{\sigma} at R_\theta \le \frac{w}{2}, y = 0 \tag{8}$$

$$P_y = \bar{P}_y + \frac{4}{\sqrt{3}}\bar{\sigma} at R_\theta = \frac{w}{2}, y = 0 \tag{9}$$

At (y= 0 and 0 ≤ Rθ ≤ w/2) the compressive stress in the Y direction of Fig. 3 is given by $\bar{P}_y$ This stress depends on the flow condition of the metal in the mandrel splines above the plane y = 0. The stress $\bar{P}_y = 0$ when the metal just crosses the plane y = 0 but at all time $\bar{P}_y = 0$.

Integration of Eq. (6) substitution of the yield condition of Eq. (8) results in:

$$\frac{P_y}{\bar{\sigma}} = \left(\frac{\bar{P}_y}{\bar{\sigma}} + \frac{4}{\sqrt{3}}\right) e^{\left(\frac{2\mu}{t_o}\right)\left(\frac{R_\theta}{2}\right) - \left(\frac{W}{2}\right)} \tag{10}$$

$$\mu = \frac{\bar{\sigma}}{\sqrt{3P_y}} \cong 0.3 - 0.6 \tag{11}$$

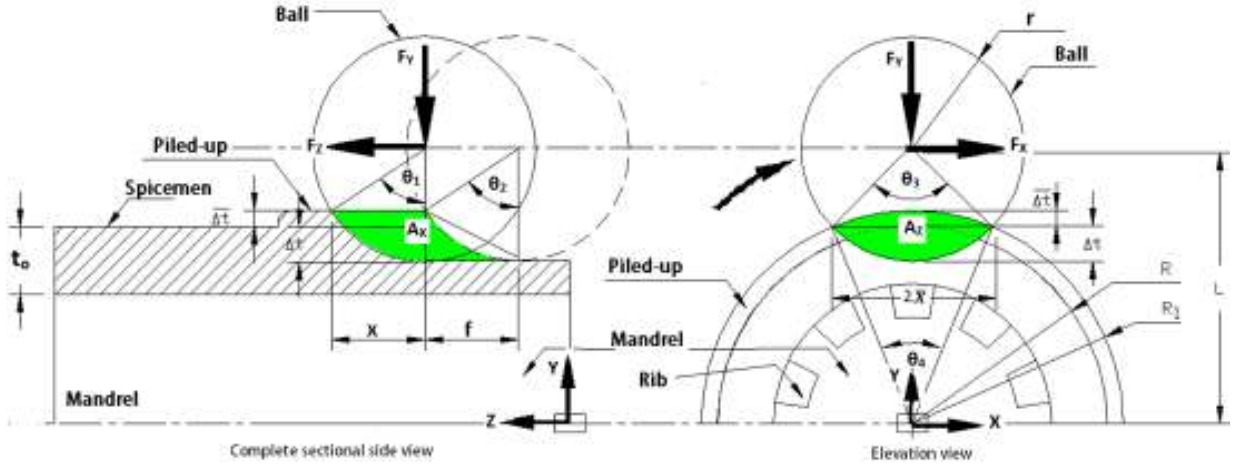

Fig. 4: Engineering drawing of projected area for ball impress in specimen

$$\frac{P_y}{\bar{\sigma}} = \frac{2}{\sqrt{3}} e^{\frac{2\mu}{w}g+1} e^{\left(\frac{2\mu}{t_o}\right)\left(\frac{R_\theta}{2}\right)-\left(\frac{W}{2}\right)} \quad (12)$$

$$\theta = \left(\frac{\pi}{180}\right)\left(\frac{360}{N}\right) \quad (13)$$

From Eq. (12), the theoretical load can be computed for forming the splines at the circumferential θ and perpendicular Y directions. The longitudinal component of the load in Z direction can be neglected. The coining loads components given by the following:

$$F_{XI} = F_{YI} = \frac{2}{\sqrt{3}}\bar{k}\sqrt{\left(\frac{1}{2}\ln\left(\frac{t_e}{t_i}\right)\right)^2 + \left(\ln\left(\frac{d_i}{d_o}\right)\right)^2}$$

$$\frac{t_e + f\sin\alpha_1}{t_i - (t_e + f\sin\alpha_1)} \quad (14)$$

$$\ln\frac{t_i}{(t_e + f\sin\alpha_1)} e^{\frac{2\mu}{w}g+1} e^{\left(\frac{2\mu}{t_o}\right)\left(\frac{R_\theta}{2}\right)-\left(\frac{W}{2}\right)}$$

$$FZI = 0 \quad (15)$$

II- For the second part of the force (shear flow of sleeve metal layer force or spinning force) can be expressed as follows:

The stress normal to the contact surface between ball and sleeve can be designated as P. The normal force acting on the contact area A is given by:

$$F = Pa * A \quad (16)$$

where, A is the direction projected area of the sphere segment. The spinning loads components can be expressed by:

$$\begin{aligned} FXII &= Pa\ AX \\ FYII &= Pa\ AY \\ FZII &= Pa\ AZ \end{aligned} \quad (17)$$

Where Pa is average contact deformation pressure and it's expressed by:

$$\frac{P_a}{\bar{\sigma}} = \frac{t_{eo}}{(t_i - t_{eo})} ln\frac{t_i}{t_{eo}} \quad (18)$$

where, $\bar{\sigma}$ is average tensile stress and it's expressed as:

$$\bar{\sigma} = \frac{2}{\sqrt{3}}\bar{k}\sqrt{\left(\frac{1}{2}ln\left(\frac{t_e}{t_i}\right)\right)^2 + \left(ln\left(\frac{d_i}{d_o}\right)\right)^2} \quad (19)$$

$$P_a = \frac{2}{\sqrt{3}}\bar{k}\sqrt{\left(\frac{1}{2}ln\left(\frac{t_e}{t_i}\right)\right)^2 + \left(ln\left(\frac{d_i}{d_o}\right)\right)^2}\left(\frac{t_{eo}}{t_i - t_{eo}}\right)\left(ln\frac{t_i}{t_{eo}}\right) \quad (20)$$

$$t_{eo} = (t_e + f\ sin\ \alpha_1) \quad (21)$$

According Hayama (1966) and the author's [10] the actual deformation ratio can be written as:

$$\begin{aligned} \bar{\varepsilon}_o &= \varepsilon_o(1 + k\ \sin\alpha_1), k = 1.2 \\ \bar{\varepsilon}_o &= \varepsilon_o(1 + 1.2\ \sin\alpha_1) \end{aligned} \quad (22)$$

$$\overline{\Delta t} = \frac{1.2\,\Delta t}{t_o}\sin\alpha_1 \quad (23)$$

$$\alpha_1 = 2\ tan^{-1}\frac{\Delta t}{R} \quad (24)$$

During the process, contact surfaces appear between the balls and the blank tube, instantaneously, this contact area maintain constant, in the respect the process might be considered as quasi-stationary. The intersection of the sphere with the circumferential surface created by ball. Such a surface is difficult to describe analytically [26]. However, the determination of its projected areas proves to be useful for further calculation of force components. Engineering drawing of projected area for ball impress in specimen shown in Fig. 4. The projected areas of this part of a sphere segment are determined by three areas in three axis.

Fig. 5: SAMPLES of internally- spline sleeves and cross section of it's at various cross in-feed

Referring to the Fig. 4, the three direction projected area of segment sphere between the ball and the specimen can be compute as the following:

$$A_X = \frac{1}{2}r^2\left(\frac{2\theta_1 - \sin(2\theta_1)}{2}\right) + \left(\frac{1}{2}\left(f(\Delta t + \overline{\Delta t})\right)\right) - r^2\left(\frac{\theta_2 - \sin\theta_2}{2}\right) \quad (25)$$

$$A_y = \left(\frac{\pi * X * \bar{X}}{2}\right) \quad (26)$$

$$A_Z = r^2\left(\frac{\theta_3 - \sin\theta_3}{2}\right) + {R_1}^2\left(\frac{\theta_4 - \sin\theta_4}{2}\right) \quad (27)$$

where, A_X is projected area in direction X, A_Y is projected area in direction Y and A_Z is projected area in direction Z as shown in Fig. 4 and θ_1, θ_2, θ_3, $\theta_4$are contact angles and its express as:

$$\theta_1 = sin^{-1}\frac{X}{r} \quad (28)$$

$$\theta_2 = sin^{-1}\frac{f}{r} \quad (29)$$

$$\theta_3 = 2\,sin^{-1}\frac{\bar{X}}{r} \quad (30)$$

$$\theta_4 = 2\,sin^{-1}\frac{X}{R_1} \quad (31)$$

where, X, $\bar{X}$ are distance shown in Fig. 5 and its express as:

$$X = \sqrt{r^2 - (R_1 - L)^2} \quad (32)$$

$$\bar{X} = \sqrt{{R_1}^2 - \left(\frac{{R_1}^2 + L^2 - r^2}{2L}\right)^2} \quad (33)$$

where, R_1 is outside radius of sleeve after piled-up and it's defined by:

$$R_1 = R + \overline{\Delta t}$$

where, R is outside radius of tube blank and Δt is the cross in feed. The distance between the center of ball and the center of the specimen defined by:

$$L = R + r - \Delta t \quad (34)$$

where, r is the radius of the forming ball.
By substituting Eq. (18), (19), (20) and 21 in Eq. (17):

$$F_{XII} = \frac{2}{\sqrt{3}}\bar{k}\sqrt{\left(\frac{1}{2}\ln\left(\frac{t_e}{t_i}\right)\right)^2 + \left(\ln\left(\frac{d_i}{d_o}\right)\right)^2}\left(\frac{t_{eo}}{t_i - t_{eo}}\right)\left(\ln\frac{t_i}{t_{eo}}\right) * \left(\frac{1}{2}r^2\left(\frac{2\theta_1 - \sin(2\theta_1)}{2}\right) + \left(\frac{1}{2}\left(f(\Delta t + \overline{\Delta t})\right)\right) - r^2\left(\frac{\theta_2 - \sin\theta_2}{2}\right)\right) \quad (35)$$

$$F_{YII} = \frac{2}{\sqrt{3}}\bar{k}\sqrt{\left(\frac{1}{2}ln\left(\frac{t_e}{t_i}\right)\right)^2 + \left(ln\left(\frac{d_i}{d_o}\right)\right)^2}\left(\frac{t_{eo}}{t_i - t_{eo}}\right)\left(ln\frac{t_i}{t_{eo}}\right) * \left(\frac{\pi\bar{X} * X}{2}\right) \quad (36)$$

$$F_{ZII} = \frac{2}{\sqrt{3}}\bar{k}\sqrt{\left(\frac{1}{2}ln\left(\frac{t_e}{t_i}\right)\right)^2 + \left(ln\left(\frac{d_i}{d_o}\right)\right)^2}\left(\frac{t_{eo}}{t_i - t_{eo}}\right)\left(ln\frac{t_i}{t_{eo}}\right) * \left(r^2\left(\frac{\theta_3 - \sin\theta_3}{2}\right) + {R_1}^2\left(\frac{\theta_4 - \sin\theta_4}{2}\right)\right) \quad (37)$$

By substituting Eq. (14), (15), (35), (36) and (37) in Eq. (1), (2) and (3):

$$F_X = F_{XI} + F_{XII} = \left[\frac{2}{\sqrt{3}}\bar{k}\sqrt{\left(\frac{1}{2}ln\left(\frac{t_e}{t_i}\right)\right)^2 + \left(ln\left(\frac{d_i}{d_o}\right)\right)^2}\frac{t_e + f\sin\alpha_1}{t_i - (t_e + f\sin\alpha_1)} \; ln\frac{t_i}{(t_e + f\sin\alpha_1)}e^{\frac{2\mu}{w}g+1}e^{\left(\frac{2\mu}{t_o}\right)\left(\frac{R_\theta}{2}\right) - \left(\frac{W}{2}\right)}\right] + \left[\frac{2}{\sqrt{3}}\bar{k}\sqrt{\left(\frac{1}{2}ln\left(\frac{t_e}{t_i}\right)\right)^2 + \left(ln\left(\frac{d_i}{d_o}\right)\right)^2}\left(\frac{t_{eo}}{t_i - t_{eo}}\right)\left(ln\frac{t_i}{t_{eo}}\right) * \left(\frac{R^2}{2}\left(\frac{\theta_1 - \sin\theta_1}{2}\right)\right)\right] \quad (38)$$

$$F_Y = F_{YI} + F_{YII} = \left[\frac{2}{\sqrt{3}}\bar{k}\sqrt{\left(\frac{1}{2}ln\left(\frac{t_e}{t_i}\right)\right)^2 + \left(ln\left(\frac{d_i}{d_o}\right)\right)^2}\frac{t_e + f\sin\alpha_1}{t_i - (t_e + f\sin\alpha_1)} \; ln\frac{t_i}{(t_e + f\sin\alpha_1)}e^{\frac{2\mu}{w}g+1}e^{\left(\frac{2\mu}{t_o}\right)\left(\frac{R_\theta}{2}\right) - \left(\frac{W}{2}\right)}\right] + \left[\frac{2}{\sqrt{3}}\bar{k}\sqrt{\left(\frac{1}{2}ln\left(\frac{t_e}{t_i}\right)\right)^2 + \left(ln\left(\frac{d_i}{d_o}\right)\right)^2}\left(\frac{t_{eo}}{t_i - t_{eo}}\right)\left(ln\frac{t_i}{t_{eo}}\right) * \left(\frac{\pi\bar{X} * X}{2}\right)\right] \quad (39)$$

$$F_Z = F_{ZI} + F_{ZII} = \left[\frac{2}{\sqrt{3}}\bar{k}\sqrt{\left(\frac{1}{2}ln\left(\frac{t_e}{t_i}\right)\right)^2 + \left(ln\left(\frac{d_i}{d_o}\right)\right)^2}\left(\frac{t_{eo}}{t_i - t_{eo}}\right)\left(ln\frac{t_i}{t_{eo}}\right) * \left({R_1}^2\left(\frac{\theta_2 - \sin\theta_2}{2}\right) + R^2\left(\frac{\theta_3 - \sin\theta_3}{2}\right)\right)\right] \quad (40)$$

The deformation loads components can be calculated from the Eq. (38), (39), (40). The required data for calculations are listed in Table 1.

Table 1: Parameters of calculation of spinning force components

No.	Parameter	Symbol	Unit	Value
1	Strength coefficient	k	Mpa	141
2	Initial sleeve wall thickness	ti	Mm	5 mm
3	Theoretical reduction in wall thickness	Δt	Mm	1.5- 3 mm
4	Outside diameter of the mandrel	Dm	Mm	30
6	Axial feed rate	f	mm/rev	0.3 -1.21
7	Coefficient of friction	μ		0.3

MATERIALS AND METHODS

The test rig components of forming process are shown in Fig. 6. The device is mounted over a conventional center lathe carriage and is adjusted concentric with its centerline. Rotation of the threaded adjusting shaft is transferred to radial movement of the forming balls through conical jaws. Each full turn of the screw is resulted in 2.0 mm axial movement of conical jaws and 0.73 mm radial movement of the forming balls. A dial gauge with 0.01 mm sensitivity was placed on the adjusting shaft to define the forming depth. The material of the tubular blank is commercial Aluminum with yield strength σ_y = 92 MPa, strength coefficient K = 141 MPa and strain hardening exponent n = 0.18 from experimental tension test. The tube blank was support axially by the mandrel shoulder and rotated by the mandrel splines. The device has three forming balls with 20.0 mm diameter made of hardened tool steel seated over carbide seats. The rotating splined mandrel was clamped to the lathe chuck at one end and the work-piece insert to the other end.

The deforming loads were measured by the dynamometer connected with data logger device through a transducer. The surface roughness of the product was measured by (SURFTEST SJ-310). The filling ratio was calculated as follows:

Table 2: Experiments plan and operating conditions

Investigation parameters	The value
Mandrel rotational speed, N	76, 150, 230 and 305 rpm
Axial feed, f	0.3, 0.6, 0.91 and 1.21 mm/rev.
Cross in-feed, Δt	1.5, 2, 2.5, 3 and 3.5 mm
Initial sleeve thickness, t	4, 5, 6 and 7 mm

- Theoretical geometry (complete filling) was calculated from the spline dimensions
- Obtained contour of formed parts is magnified to a predetermined scale using a microscope to calculate the actual volume filled.

The filling ratio is computed as the following:

$$FR = \frac{\text{actual volume of internal ribs}}{\text{theoretical volume of mandrel cavity}} = \frac{\text{actual area of internal rib} * \text{sleeve length}}{\text{theoretical area of mandrel cavity} * \text{sleeve length}} \quad (41)$$

A photo scan for the mandrel and formed workpiece is illustrated in Fig. 3. The actual and theoretical areas were computed using by AutoCAD program.

The sets of experiments has been performed, the effect of the process parameters (t, Δt) and machine parameters (f, N) on the deformation loads were examined as a function of the cross in-feed, axial feed and tube thickness. In other sets of experiments, the influence of the process and machine parameters on the sleeve product quality was investigated as a function of the cross in-feed, axial feed and tube thickness. The product quality presented in surface roughness and filling ratio of the internal splines. Table 2 illustrates the experiments plan and operating conditions.

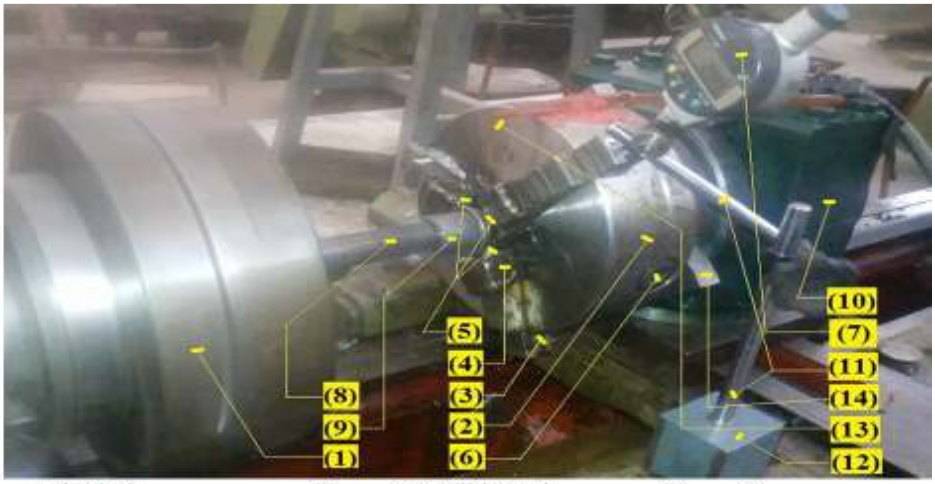

(1) Lathe Chuck (2) New Ballizing Tool (3) Jaw
(4) Ball Holder (5) Forming Balls (6) Adjusting Screw
(7) Dial Gauge Indicator (8) Mandrel (9) Specimen
(10) Dynamometer (11) Connection (12) Fixture

Fig. 6: Experimental set-up of the deforming process

RESULTS AND DISCUSSION

Internally-splined sleeves product: The internally-splined sleeves product for different cross in-feed, at 230 rpm mandrel rotational speed are shown in Fig. 5. It is clearly shown that the internally-splined sleeves product can be deformed by a ball-shaped rotary tool ballizing process. This result is compatible with (Shuyong, 2008) who included that the ball shaped tool can be used in this process.

Effects of the process parameters on the forming load: The measured radial and tangential components of the deformation load have been plotted versus the cross in-feed at various speeds and axial feed as in Fig. 7. In general. The forces seem to be increase slightly with the increase of the cross in-feed. The force action can be interpreted by that the balls are actually penetrating in the material and acting within the material in bulk underneath material of the outside layer of the aluminum sleeve. Increasing the cross in-feed more than 2.5 mm causes piled-up metal, this is due to increasing the contact area with the increase of axial feed, hence, the bill up was increased also this raises the forming load components.This means that the deformation ratio was increased more than. The mentioned result is in accordance with (Jiang *et al*., 2009b; El-Sheikh, 1991). The deformation load is essentially needed for forcing the material to penetration into the mandrel splines and to displace or to squeeze the piled-up metal form the front of the rotating advanced balls. Figure 7 illustrates also that, an increasing the axial feed rate which causes a significant increase in the deformation load. This is due to the appearance of screw formed waviness the surface.

Figure 8 shows that, the increasing of mandrel speed is corresponded by a decrease in the maximum deformation load until it reaches its minimum value at the optimum mandrel speed. It is raised again with the increase of the mandrel speed above its optimum value, this is may be due to the metal flow rate cause change in forming load, at low speed the metal flow rate is higher this lead to the forming load increase and at high speed the metal flow conform with rotational speed to reach to the minimum value of load at best speed. The increase in rotational speed above this value the intentness strain hardness for Aluminum tube this lead to increase forming load.

Effects of the Process parameters on the filling ratio of splines: Figure 9 shows the percentage difference between the formed internal sleeve splines and the rotating mandrel splines cross sections. This difference decreases with the increase of the cross in-feed and

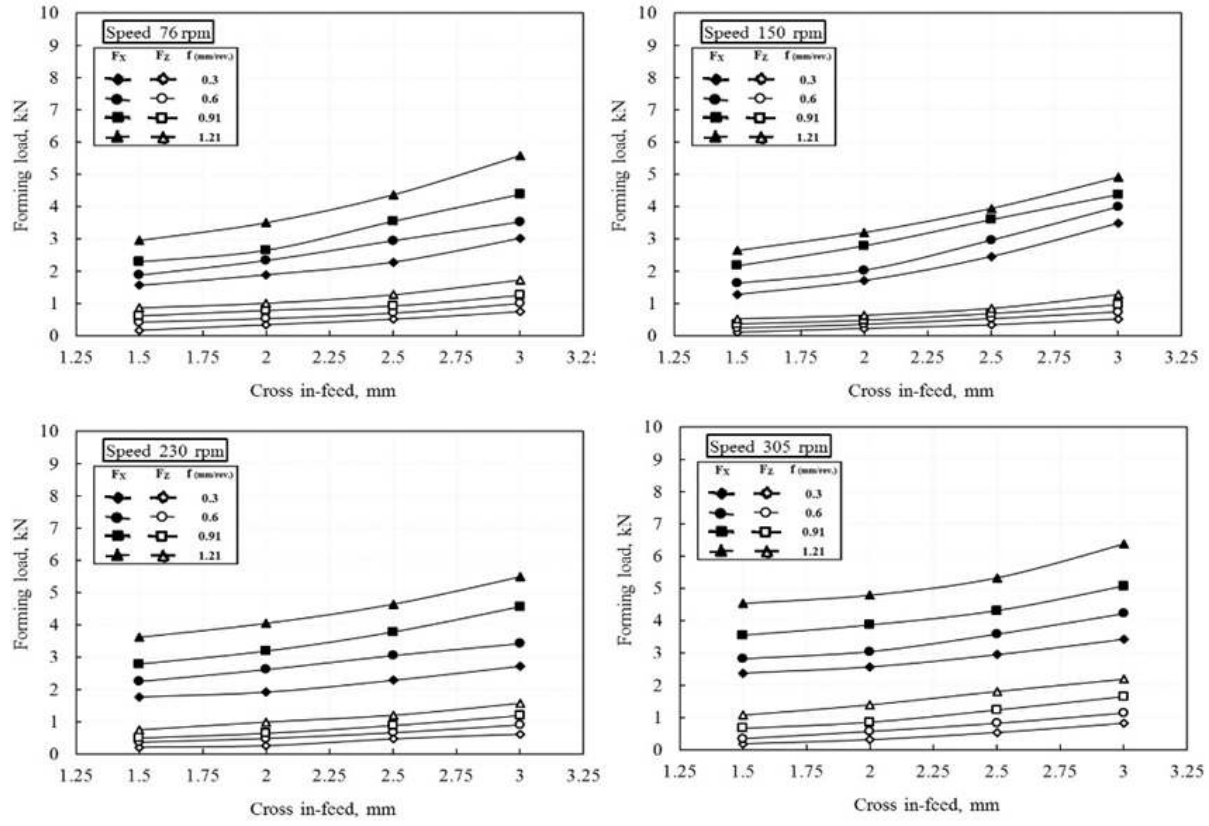

Fig. 7: Maximum forming load versus cross in-feed relation

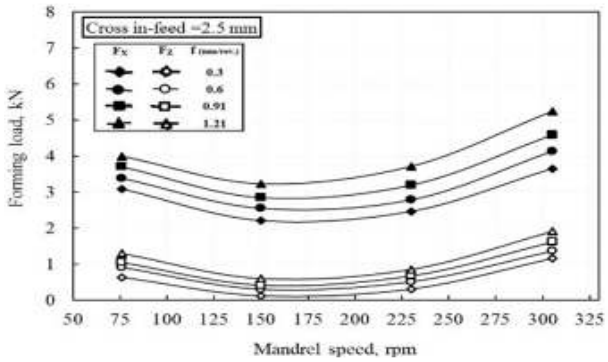

Fig. 8: Maximum load rotational mandrel speed relation at cross in-feed 2.5 mm

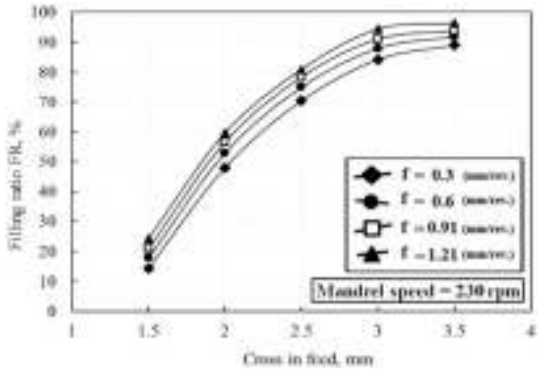

Fig. 9: Effect of cross in-feed on the deforming splines

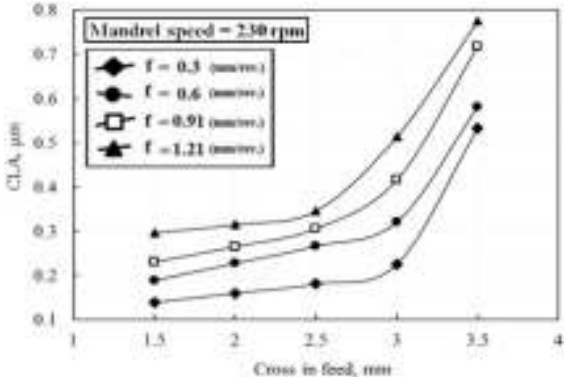

Fig. 10: Effect of cross in-feed on CLA

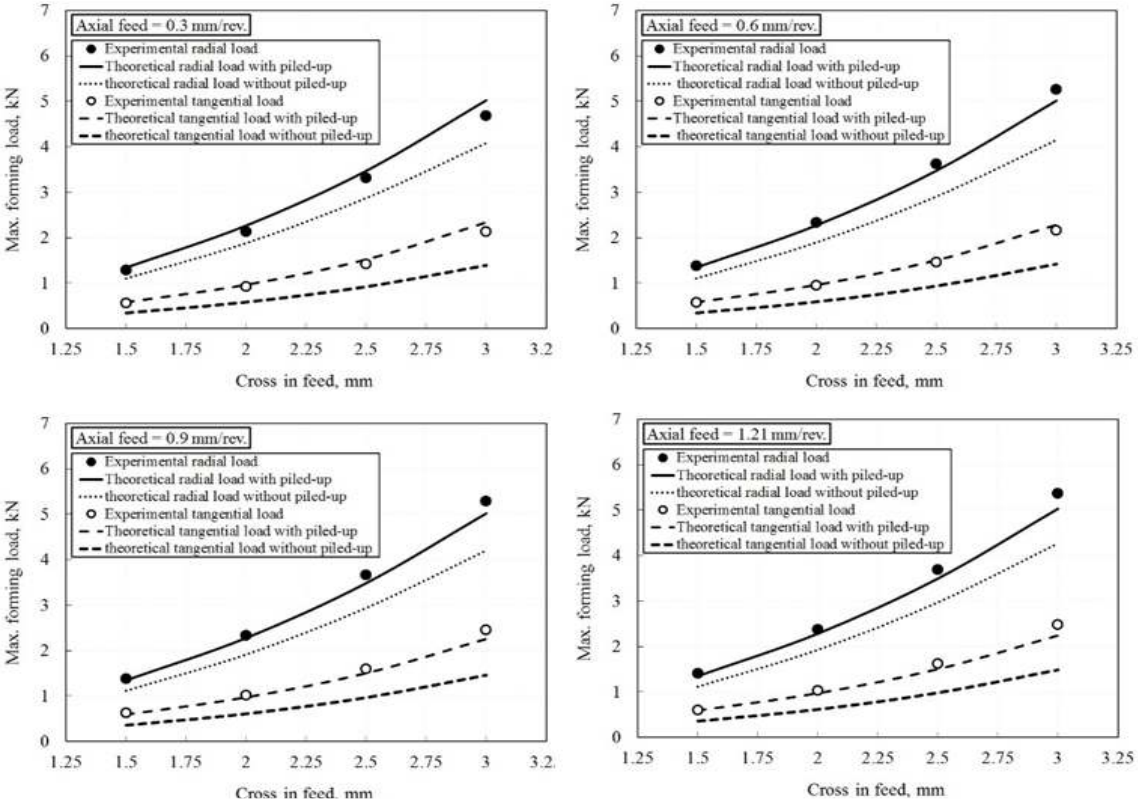

Fig. 11: A comparison between computed results and experimental data at axial feed 0.3, 0.6, 0.9 and 1.21 mm/rev

reaches its minimum value at 3 mm cross in-feed. With the increase of the cross in-feed above 3 mm, deterioration of the external metal sleeve occurs. Figure 9 shows also the cross section of the internally spline sleeves at different axial feed and cross in-feed at speed 230 rpm.

The variation of center line-average CLA of the surface roughness and cross in-feed at various axial feed rate and constant rotational mandrel speed are shown in Fig. 10. Figure illustrates also the center line-average CLA of the surface roughness having minimum values at the optimum mandrel speeds. The generation of sleeve vibration during the deformation process due to the increase of the rotational mandrel speed is accompanied by an increase in the center line-average CLA of the surface roughness. Prakash and Singhal (1995) illustrated that the achieved concentricity of the product was about 8% which is commercially acceptable but with the new tool design used in this research the achieved concentricity was about 0.02% of the wall thickness.

Comparison between computed and experimental results: The theoretical and experimental deforming load values at the optimum mandrel rotational speed are shown in Figure 11. The theoretical forming loads were calculated with and without pile up. It has been noticed that by increasing the cross in-feed, a significant difference occurs between the theoretical and experimental values this is due to the appearance of pile up deformed metal in front of the balls.

CONCLUSION

From the experimental results and theoretical analysis the following conclusions can be drawn:

- Mandrel rotational speed, axial feed and cross in-feed have remarkable effects on the forming load and the product quality.
- The results from the derived analytical (forming load) two cases, with and without pile up, the results with pile up formation have were to be in close agreement with the experimental results.
- The surface roughness of sleeve improved with the increasing of cross in-feed. But, derogated with increasing of the axial feed.
- The filling ratio improved with increasing the cross in-feed and axial feed

ACKNOWLEDGMENT

The authors would like to thank Eng. A. Atia and Eng. E. Kh. Saied whom have been of great help in the experimental work.

Funding information: This study was supported by BENI-SUEF University, Scientific Research Development unit, Projects Funding and Granting Unit.

REFERENCES

Ahmed, K.I.E., 2011. A new ball set for tube spinning of thin-walled tubular parts with longitudinal inner ribs. J. Eng. Sci. Assiut Univ., 39(1): 15-32.

El-Sheikh, M.N., 1991. A new developed technique in deformation of internal splines. Bull. Facult. Eng., 4: 120-135.

Groche, P. and D. Fritsche, 2006. Application and modelling of flow forming manufacturing processes for internally geared wheels. Int. J. Mach. Tool. Manu., 46(11): 1261-1265.

Hayama, M., 1966. Theoretical study of tube spinning. Bull. Fac. Eng. Yokohama Univ., 15: 33-47.

Jiang, S., Z. Ren, C. Li and K. Xue, 2009a. Role of ball size in backward ball spinning of thin-walled tubular part with longitudinal inner ribs. J. Mater. Process. Tech., 209(4): 2167-2174.

Jiang, Y.S., Y.F. Zheng, Z.Y. Ren and C.F. Li, 2009b. Multi-pass spinning of thin-walled tubular part with longitudinal inner ribs. T. Nonferr. Metal. Soc., 19(1): 215-221.

Kuss, M. and B. Buchmayr, 2016. Damage minimised ball spinning process design. J. Mater. Process. Tech., 234: 10-17.

Liu, J.S. and X.P. Wang, 2013. Research in optimization of inner-grooved copper tubes forming. Adv. Mater. Res., 641-642: 591-594.

Prakash, R. and R.P. Singhal, 1995. Shear spinning technology for manufacture of long thin wall tubes of small bore. J. Mater. Process. Tech., 54(1-4): 186-192.

Shu-Yong, J., X. Kemin, L. Chunfeng and R. Zhengyi, 2006. Spinning deformation criteria of thin-walled tubular part with longitudinal inner ribs. J. Wuhan Univ. Technol. Mater. Sci. Ed., 21(4): 169-172.

Shuyong, J., 2008. Analysis of mechanics in ball spinning of thin-walled tube. Chinese J. Mech. Eng., 21(1): 25-30.

Tang, Y., Y. Chi, J.C. Chen, X.X. Deng, L. Liu, X.K. Liu and Z.P. Wan, 2007. Experimental study of oil-filled high-speed spin forming micro-groove fin-inside tubes. Int. J. Mach. Tool. Manu., 47(7-8): 1059-1068.

Wong, C.C., T.A. Dean and J. Lin, 2003. A review of spinning, shear forming and flow forming process. Int. J. Mach. Tool. Manu., 43(14): 1419-1435.